physical meaning is that, upon axial coordination, the direction of the unique axis can switch from the normal to the macrocyclic plane to the direction of the strongest metal–ligand bond, i.e. to the metal–isoindole nitrogen direction. Simultaneously the electronic structure changes from rhombically elongated to rhombically compressed.

Conclusive support for this picture should come from single-crystal studies, through location of the highest and lowest *g* values along the above-mentioned directions. Unfortunately, we were not able, up to now, to obtain suitable single crystals from any of the copper-doped zinc adducts.

Conclusions

The information provided above indicates that hpH$_2$, in spite of its apparent similarity with porphyrin-like ligands, is a rather peculiar macrocycle with a coordination chemistry strongly influenced by its low aromaticity, by the inequivalence of the coordinating nitrogens, and by the weakness of its ligand field.

Compared to other macrocycle species, the M(hp) complexes appear to be low-symmetry compounds with substantial admixture of different d orbitals into the ground state. They easily coordinate axial ligands, and in the case of protic molecules, the adducts are strongly stabilized by proton–ligand

interaction with partial dissociation of the coordinated molecules. Both the 1/1 and the 1/2 adducts isolated behave as six-coordinated compounds, apparently through intermolecular association. Furthermore, the coordination of axial ligands strongly affects the electronic structure of the M(hp) complexes, as shown by the ground-state changes that occur for the two quasi-degenerate Co(II) and Cu(II) compounds. Upon axial coordination Co(hp) goes from low- to high-spin configuration and Cu(hp) may change from a rhombically elongated to a rhombically compressed electronic structure.

Besides the preparation of crystals suitable for X-ray analysis current work is now aimed at the characterization of hpH$_2$ complexes with different metal ions and at the study of their reactivity with small molecules.

Contribution from the Department of Chemistry and Materials Science Center, Cornell University, Ithaca, New York 14853

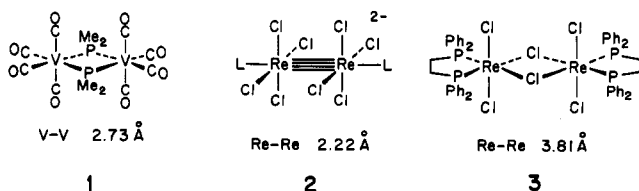# Marcasites and Arsenopyrites: Structure, Bonding, and Electrical Properties

SUNIL D. WIJEYESEKERA and ROALD HOFFMANN*

The structure of marcasite is discussed in terms of infinite chains of trans-edge-sharing octahedra. Distortion of these chains along their axes is considered. In d^6 marcasite, filled-shell repulsion of the ligand backbone keeps the metal atoms apart. In contrast, a uniform shortening of the chain axis for electron count d^4 is seen to result in partial ligand–ligand bond formation (P–P = 2.7 Å in FeP$_2$) as well as the expected metal–metal bonding. The contraction from d^6 geometry is shown to occur due to the emptying of a P–P σ^* orbital early along the reaction coordinate. M–M, L–L, and M–L interactions all work together to produce a band gap for the d^4-contracted chain. Arsenopyrite is the result of a pairing distortion (d^5). It is a semiconductor, for the same reason as d^1 NbCl$_4$ is. The optimal electron count at which pairing occurs is related to the nature of the ligand in marcasite, rutile, NbCl$_4$, and model intermediates.

Given a ratio of elements subjected to a certain temperature and pressure, what will come out of a flask? That, incredibly enough, is the question posed by solid-state chemists. Clearly the theoretician can come nowhere near an answer, but it is possible he or she could answer questions of preference for one of a few closely related structures. What do we mean by closely related? It seems reasonable to look for analogies from the comparatively well-understood world of molecules.

Recently, Shaik, Hoffmann, Fisel, and Summerville[1] studied compounds **1–3**. Each of these M$_2$L$_{10}$ compounds has the

V–V 2.73 Å   Re–Re 2.22 Å   Re–Re 3.81 Å

1   **2**   **3**

same octahedral coordination around the metal and the same

(1) Shaik, S.; Hoffmann, R.; Fisel, C. R.; Summerville, R. H. *J. Am. Chem. Soc.* **1980**, *102*, 4555–4572.

Table I. Distortions as a Function of Electron Count in Some Edge-Sharing Octahedral Structures

structure type	electron count		
	uniform expansion	pairing distortion	uniform contraction
NbCl$_4$[2,13]	d^4	d^1 (d^2?)	
rutile (MO$_2$)[14]	d^4, d^5	d^1, d^2, d^3	
marcasite (ML$_2$)[21d] (L = P–Bi, S–Te)	d^6	d^5	d^2, d^4

electron count, d^4. But, what a difference in M–M distance results from changing the ligand in these three compounds.

An obvious extension of the M$_2$L$_{10}$ edge-sharing compounds to infinity is chain **4** in which octahedra share only trans edges. Three well-known structures, NbCl$_4$, rutile, and marcasite, contain such chains. As in the case of the molecules, contractions perpendicular to the shared edges can occur, leading to shorter M–M distances.

Now, however, this contraction can have any periodicity within the infinite chain. Table I lists data for these compounds, for electron counts d^6 and below, and for the extreme periodicities consisting of the uniform contraction **5** and the

4

$\theta = 90°$

5

$\theta < 90°$

6

$\theta_1 < 90°$
$\theta_2 > 90°$

X	$r_{Nb,Nb}$	$r'_{Nb,Nb}$
Cl	3.794	3.029 Å
I	4.36	3.31 Å

7

pairing distortion **6**. Contraction and expansion are calibrated with use of the angle θ at the bridging ligand shown in **4**. $\theta < 90°$ would then be a contraction.

It might appear that a structural deformation this simple would be easily understood. In fact, Whangbo and Bullett independently did band calculations on the pairing distortion that is undergone by $NbCl_4$.[2a,b] Shaik has studied a trimer model for $NbCl_4$.[2c] There also exist a large number of calculations on the expanded (metallic) form of rutile.[3] So why do we need more band calculations? First, Table I shows that marcasite is very different from $NbCl_4$. It undergoes a uniform contraction (d^2, d^4). Pairing occurs for an electron count (d^5) that is different from that of $NbCl_4$. However, the only band structure of marcasite, due to Bullett,[4] does not consider structural deformation at all. It concentrates on explaining the photoelectron spectrum of d^6 "expanded" marcasite, which it does very well.

Hence, one motivation for this study is the understanding of the relationship among structure type, structural deformation, and electron count. An important reason for studying such structural deformations is that they relate to the electrical properties of the solid. After a pairing distortion, every other metal to metal contact is long. This reduces conductivity along the chain axis and can lead to semiconducting behavior. Hence, it is important to be able to predict when such a distortion occurs.

The uniform contraction implies a continuous chain of overlapping metal orbitals. It is thus a major surprise that d^4 marcasite is a diamagnetic semiconductor, and as we shall describe later, a lot of experimental and theoretical effort has gone into trying to explain this fact.

Structure

The infinite chain **4**, in which all equatorial ligands are shared between two octahedra, has stoichiometry ML_4. $NbCl_4$ **7**, which has the same stoichiometry, consists of essentially isolated chains of type **4**, or rather **6**.

Rutile and marcasite have stoichiometry ML_2. This stoichiometry can be achieved by removing all axial ligands in **4**.
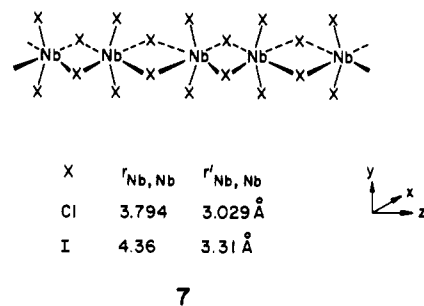
One way in which octahedral site symmetry can be regenerated without changing stoichiometry is shown in **8**. One chain,

8
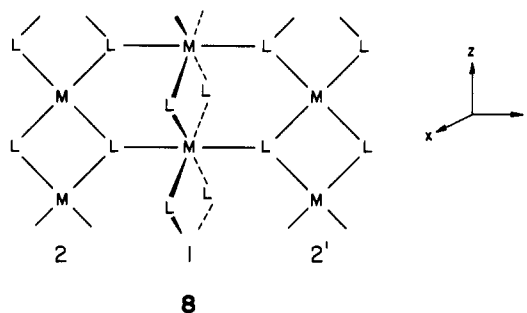
chain 1, has been rotated by 90° and moved up half a unit cell along the z axis. As a result, equatorial ligands on chains 2 and 2′ become axial ligands on chain 1. Regeneration of octahedral site symmetry on chains 2 and 2′ requires interaction with chains parallel to chain 1 but lying above and below the plane of the paper. Continuing, an infinite three-dimensional network, rutile, is built up.

9 emphasizes the environment about a metal atom in rutile.

9
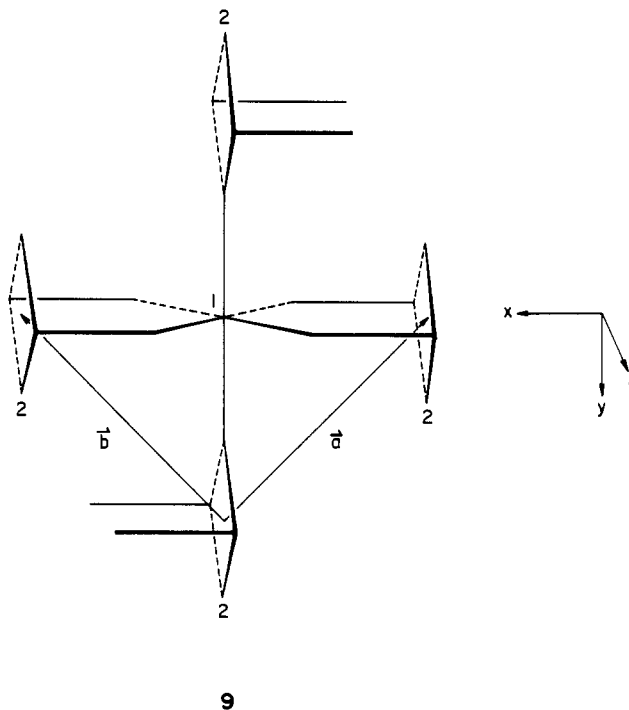
A chain of type 1 is surrounded by four chains of type 2. The unit cell axes shown imply the presence of two ML_2 units per unit cell, displaced from one another by the vector $(^1/_2, ^1/_2, ^1/_2)$. A rotation of 90° about the origin and a translation of $(^1/_2, ^1/_2, ^1/_2)$ take a chain of type 2 into a chain of type 1 and vice versa. Hence, a C_4 axis exists; in fact the full symmetry of the solid including nonsymmorphic operations may be seen to be D_{4h}^{14}.[5] The point symmetry at the metal is C_{2h}.

(2) (a) Whangbo, M.-H.; Foshee, M. J. *Inorg. Chem.* **1981**, *20*, 113–118. (b) Bullett, D. W. *Ibid.* **1980**, *19*, 1780–1785. (c) Shaik, S. S.; Bar, R., submitted for publication.

(3) Not including band structures on TiO_2: (a) Gupta, M.; Freeman, A. J.; Ellis, D. E. *Phys. Rev. B: Solid State* **1977**, *16*, 3338–3351. (b) Posternak, M.; Freeman, A. J.; Ellis, D. E. *Phys. Rev. B: Condens. Matter* **1979**, *19*, 6555–6563. (c) Umrigar, C.; Ellis, D. E. *Ibid.* **1980**, *21*, 852–861. (d) Mattheiss, L. F. *Phys. Rev. B: Solid State* **1976**, *13*, 2433–2450. (e) Sasaki, T. A.; Soga, T.; Adachi, H. *Phys. Status Solidi B* **1982**, *113*, 647–655. (f) Caruthers, E.; Kleinman, L.; Zhang, H. I. *Phys. Rev. B: Solid State* **1973**, *7*, 3753–3760.

(4) Bullett, D. W. *J. Phys. C.* **1982**, *15*, 6163–6174.

**10** and **11** illustrate the transformation rutile → marcasite.
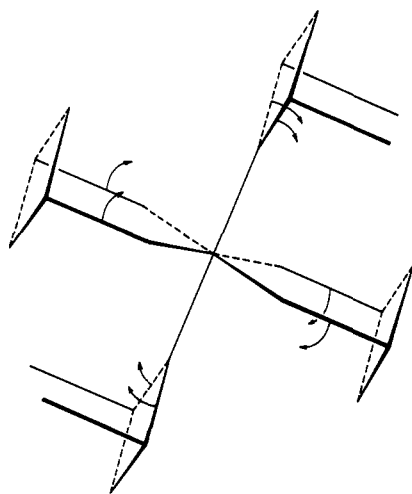
10
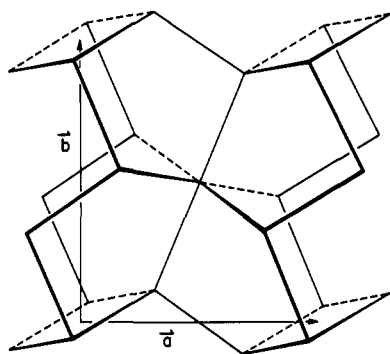
11

All ligands pyramidalize, and the arrows indicate the relative movement of some of the bonds. The net result is that planar three-coordinate ligand atoms in rutile are saturated through the formation of an extra L–L bond per ligand. The distortion rutile → marcasite and the resulting structure have the non-symmorphic symmetry D_{2h}^{12}, where the nonsymmorphic translation is $(^1/_2, ^1/_2, ^1/_2)$ for the unit cell axes shown. The closing of the L–L bond results in the formation of five-membered rings, **12**, each containing two metal and three
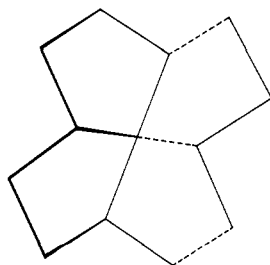

12

ligand atoms. In fact, it is possible to describe marcasite in terms of interacting nets of five-membered rings and to relate

it to the pyrite structure as well as a number of structures adopted by square-planar Pd.[6]

General Approach: Orbitals of a Model Chain

In this paper, we shall describe the bonding in marcasites and the changes that occur as the chains within distort. However, most of our work will be done not on marcasite but on the model chain **13**. This resembles the chains within
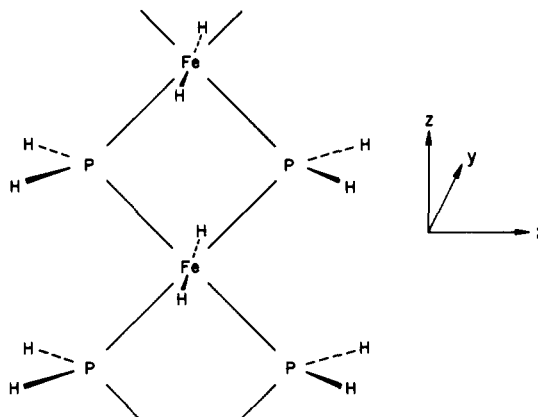
13

marcasite since equatorial P is "tetrahedrally" coordinated just as is P in marcasite. It may at first sight seem strange that the axial ligand used is H, not PH_3. This is because (i) axial PH_3's bump into one another and (ii) the ratio of the number of Fe–Fe contacts to the number of P–P contacts along the contracting axis will be seen to be important to the overall energy picture. In marcasite, axial P's of one chain are simply equatorial P's of another chain, so that the ratio is 1:2. We also note that the model chain is of interest in its own right: PH_2 is a good bridging group in inorganic chemistry, and it is possible such a chain would be synthesized in the future.

One advantage of using such a chain is that it is easier to pick out a few key orbitals. By doing so, we hope to give the experimentalist a simple, transportable picture: one that allows him to predict the properties of unknown compounds from simple "back of the envelope" calculations. Another advantage is that it is easy to model differences between marcasite, rutile, and $NbCl_4$. We simply replace the equatorial and/or axial ligands in **13** by others that have the correct local coordination of oxygen or chlorine. It is important to test the validity of such a model: the section on three-dimensional marcasite is meant to be such a test.

How do we describe the infinity of states present in a chain? One way is to go to smaller units, and of course the dimer M_2L_{10}, which was discussed by Shaik and Hoffmann (see introduction and ref 1), bears some resemblance to our study. We have chosen, instead, to start with the two high-symmetry points, $k = 0$, the zone center, and $k = 0.5$, the zone edge. This subset of chain orbitals is numerically equivalent to a fragment containing two unit cells, in which there are however interactions with the missing neighbors along the chain axis. Burdett[7] has given this fragment a name, the fragment within a solid. Although we use his very useful notation, we do not use his specific computational method in our discussion.

(5) For a description of notation in space groups see: Burns, G.; Glazer, A. M. "Space Groups for Solid State Scientists"; Academic Press: New York, 1978.

(6) (a) Brostigen, G.; Kjekshus, A. *Acta Chem. Scand.* **1970**, *24*, 2983–2992. (b) Kjekshus, A.; Rakke, T. *Struct. Bonding (Berlin)* **1974**, *19*, 85–104. (c) Burdett, J. K.; McLarnan, T. J. *Inorg. Chem.* **1982**, *21*, 1119–1128. (d) Jeitschko, W. *Acta Crystallogr., Sect. B* **1974**, *B30*, 2565–2572.

(7) Burdett, J. K. *J. Am. Chem. Soc.* **1980**, *102*, 5458–5462.
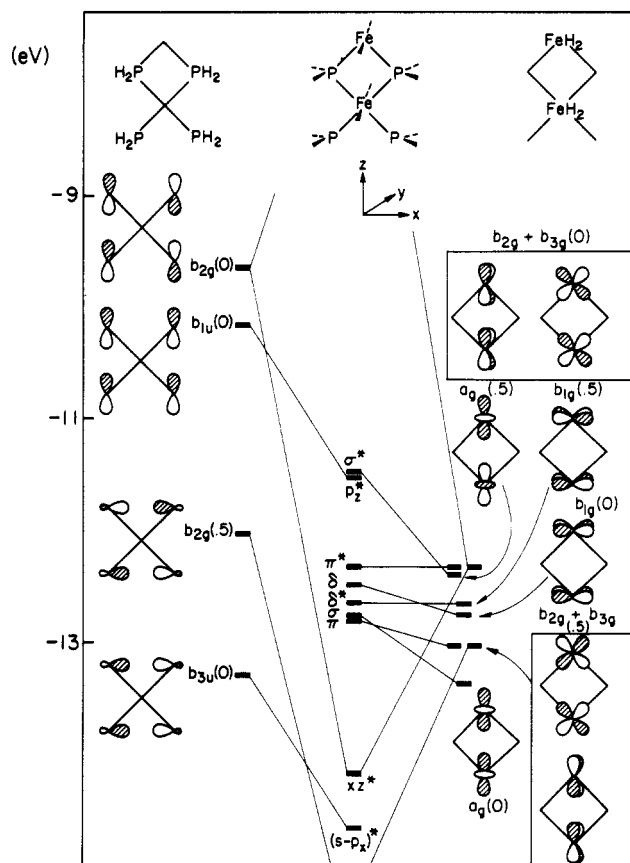
**Figure 1.** Interaction diagram for the fragment within a solid [Fe-$(PH_2)_2H_2]_2$ corresponding to the model chain at $k = 0$ and $k = 0.5$. One bonding orbital, b_{2g} (0.5) or xz is off scale.
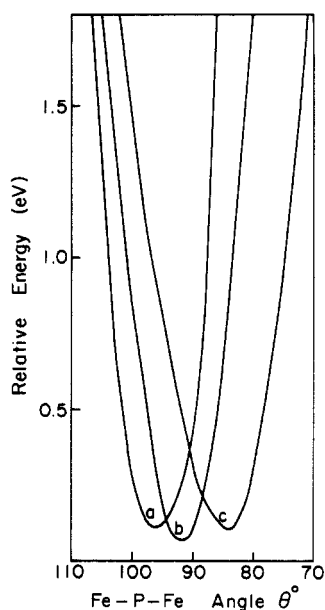
Figure 2. Relative energy curves for the uniform contraction of marcasite. The three different occupancies shown are (a) d^6, (b) d^5, and (c) d^4.

The starting point for both the uniform and nonuniform contractions is $\theta = 90°$. Figure 1 is an interaction diagram for the fragment (from now on, read fragment within a solid) [Fe($PH_2)_2H_2]_2$ built up from similar [$(PH_2)_2]_2$ and [$FeH_2]_2$ fragments. The symmetry labels used refer to the infinite chain: both its D_{2h} point symmetry (Fe as origin) and its translational symmetry (0 or 0.5). The PH_2 unit is well-known. Its HOMO's are two "lone pairs": one pure p_z and the other

an s-p_x hybrid. The highest orbitals of $(PH_2)_4$ are those combinations of the lone pairs, antibonding along the axes of their respective p orbitals. What is surprising is the extent to which these antibonding orbitals have been pushed up in energy, in two cases above the metal d orbitals. The extent of this dispersion is evident in **14**, the band structure of the [$(PH_2)_2]_∞$ chain.
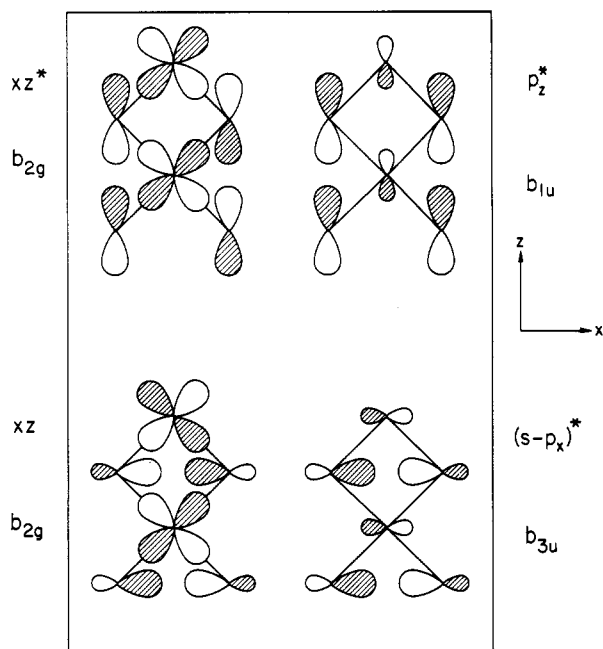

14
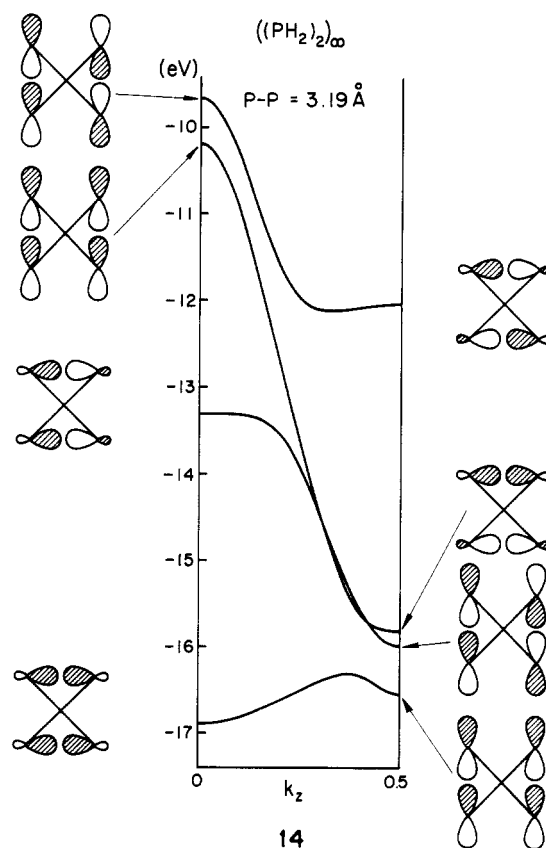
The distance between nearest-neighbor Fe atoms is the same as that between nearest-neighbor P atoms: 3.196 Å. At this distance Fe–Fe interaction is small; the splitting of orbitals on the right side of Figure 1 is about 1 eV.
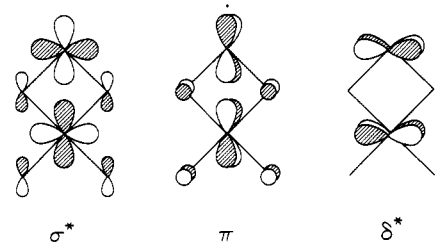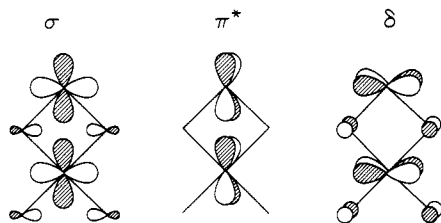
Finally, we turn on Fe–P interactions. The rules of this interaction diagram are similar to those of molecular orbital interaction diagrams: two orbitals can mix only if they have the same symmetries. However, we must consider translational as well as point group symmetry. In particular, since we have taken the metal atom as our origin, positive and negative combinations of metal xz have the same rotational symmetry, b_{2g}. **15** clearly shows that they interact with different ligand orbitals; $xz^*(0)$ interacts with phosphorus $p_z(0)$ whereas xz-(0.5) interacts with phosphorus s-$p_x(0.5)$.

This leaves eight orbitals in Figure 1 unaccounted for. The two remaining $(PH_2)_4$ orbitals are lowered by interaction with empty metal p orbitals. Since the energy match of a metal p orbital with a ligand orbital is poor, these two orbitals are lowered less than the two b_{2g} orbitals, which interact with metal xz. At this point we note the somewhat unconventional nomenclature used for the four core orbitals. The classification is indicative of their different behavior on contraction or expansion of the chain (vide infra): the b_{2g} orbitals that localize on the metal have been named xz and xz^*; the b_{1u} and b_{3u} orbitals behave like ligand σ^* orbitals and are named p_z^* and (s-$p_x)^*$, respectively.

The six remaining $(FeH_2)_2$ orbitals are classified in anticipation of M–M bonding as σ, $\sigma^*(z^2 - x^2)$, π, $\pi^*(yz)$, and δ, $\delta^*(xy)$. They constitute the t_{2g} set. They are pushed up by π bonding with the bridging ligands, **16**; the details of this interaction are more profitably considered later.
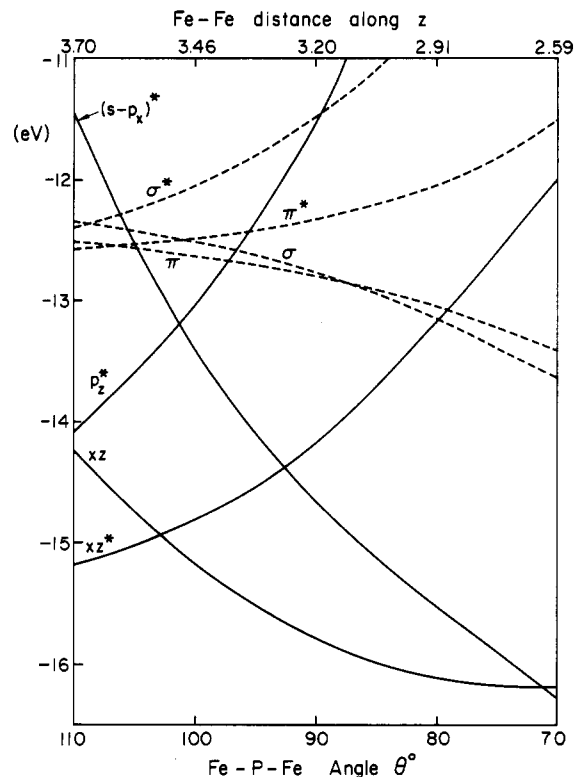
15

16

Figure 3. Walsh diagram for the "fragment within a solid" orbitals derived in Figure 1. The core orbitals (**15**) are solid, and the t_{2g} orbitals (**16**) are dashed. δ and δ^* orbitals, which have been left out, have a flat profile at 12.5 eV. The upper scale (Fe–Fe distance) is not linear.

Uniform Distortion: Total Energy and Bonding

Figure 2 shows the total energy curve obtained from an extended Hückel calculation[8] on the uniform contraction of the marcasite FeP_2 (parameters and bond lengths in Appendix I). The geometry was slightly idealized, and axial Fe–P bond lengths were set equal to equatorial ones.[9] The energy was averaged over 3 k points, a so-called special points set.[10] This set, specified in Appendix II, was chosen to emphasize dispersion along the longitudinal axis of the chain. Given that there is one P–P bond per ligand, the iron in the neutral solid

is Fe(IV), d^4. Total energy curves are shown for FeP_2, FeP_2^-, and FeP_2^{2-}. If these results are compared to the experimental results (Table II), we see good agreement in θ_{min} for d^6. The theoretical value of 84° for d^4 is considerably larger than that from experiment, but the trend is correct.

The rest of this section shall be devoted to an explanation of these energy curves. We shall first use a Walsh diagram for the orbitals derived in the previous section to explain changes in bonding (overlap population) as the chain contracts. In the process we will find several effects: these can be sorted out by comparing total energy curves for different electron counts. Finally, we consider the appropriateness of the fragment within a solid, and the chain **13**, to discussing marcasite.

Figure 3 is the Walsh diagram for the orbitals derived in Figure 1. For electron count d^6, all of the orbitals shown are filled. We see two major sources of repulsion in the fragment. The core is the more dramatic: two of the four orbitals rise in energy at low θ and the other two at high θ.[11] This corresponds to our intuition that as we decrease θ, phosphorus atoms bump into one another along the chain (z) axis and as we increase θ, there is a steric repulsion between phosphorus atoms along the x axis. There is an asymmetry in the core orbitals with respect to $\theta = 90°$. This is because overlap between the more directed p_z orbitals is greater than that between s–p_x hybrids. As a result, the minimum in the total energy moves to $\theta > 90°$.

The profile of the metal t_{2g} orbitals is much tamer. Since we have filled both bonding and antibonding orbitals, there is a barrier to contraction of the chain. The net effect of both core and t_{2g} repulsion is a minimum in Figure 1 at an elongated chain ($\theta = 97.5°$).

Table III depicts the changes in overlap population (bonding) as θ changes. The core repulsion is reflected in almost

(8) Hoffmann, R. *J. Chem. Phys.* **1963**, *39*, 1397–1412. Hoffmann, R.; Lipscomb, W. N. *Ibid.* **1962**, *36*, 2179–2195.

(9) This leaves one free parameter, the dihedral angle between the two chains in the unit cell. This was optimized at the experimental values of θ for d^6 and d^4; the amount of energy involved was small.

(10) (a) Chadi, D. J.; Cohen, M. L. *Phys. Rev. B: Solid State* **1973**, *8*, 5747–5753. (b) Monkhorst, H. J.; Pack, J. D. *Ibid.* **1976**, *13*, 5188–5192.

(11) The interested reader may compare this example to the M_2L_{10} compounds where repulsion in the bridging system only occurred at high θ.

Table II. Properties of Binary Marcasites (and Arsenopyrites)[a]

| d^n	formula	θ, deg	c, Å	$(M-L)_{ax}$, Å	$(M-L)_{eq}$, Å	L–L, Å	occurrence	electrical and magnetic properties	ref
d^2	CrSb$_2$	74.9	3.27	2.75	2.69	2.84	only CrSb$_2$	antiferromagnetic or paramagnetic	21
d^4	FeP$_2$	72.9	2.72	2.20	2.29	2.27	gp 5A with	semiconductors	21
	FeAs$_2$	74.3	2.88	2.36	2.39	2.49	transition metal		21
	FeSb$_2$	75.9	3.20	2.58	2.60	2.89			21
	RuP$_2$	74.5	2.87	2.35	2.37	2.23			21
d^5	RhP$_2$	102.0	3.67			2.24	gp 5A with	semiconductors	27a
		70.6	2.68				transition metal		
	RhSb$_2$	93.7	3.91			2.84	except CoP$_2$, Bi^{3-}		27a
		73.0	3.03						
d^6	FeS$_2$	97.2	3.39	2.24	2.26	2.22	gp 5A and 6A with	semiconductors	21
	FeSe$_2$	97.53	3.58	2.37	2.38	2.54	transition metal		21

[a] Ternary complexes occur for the mixtures d^2/d^4 and d^4/d^6.

zero P–P overlap populations; the t_{2g} repulsion, in negative Fe–Fe overlap populations.

To go from d^6 to d^4 in our fragment containing two iron atoms requires the removal of four electrons, initially from σ^* and π^*. Removal of electrons from these antibonding orbitals causes the chain to contract, turning on further M–M σ interaction. A second, crucial, reason for the contraction is that an orbital crossing early along the reaction coordinate ($\theta = 95°$) allows p_z^* to become unoccupied. Hence, there is only one occupied rising core orbital at low θ, instead of two. In terms of bonding, emptying of antibonding orbitals implies a positive overlap population, Fe–Fe or P–P, a fact which is shown in Table III.

Let us rephrase what we have just stated: the contraction is related to increased P–P bonding along the chain axis, as well as the expected increase in Fe–Fe bonding. This is a surprise, and later we will show that it is a cause of the unexpected electrical properties of this compound.

Table III also shows that on contraction Fe–P overlap population decreases. In fact, this is the only trend in bonding that does not favor contraction (for d^4). This effect can be traced to the one rising core orbital that remains occupied on contraction, xz^*. This orbital is Fe–P bonding, **15**. However, when the chain is contracted, the $(PH_2)_4$ contribution rises in energy very fast and provides a poorer energy match for the FeH_2 contribution (imagine we are turning on Fe–P interaction as in Figure 1). In addition, overlap between the Fe and P contributions decreases: this is shown pictorially in **17**.

$\theta = 90°$ $\theta = 73.36°$

17

$|S_{xz-p_z}| = 0.090$ $|S_{xz-p_z}| = 0.048$

$|S_{xz-xz}| = 0.019$ $|S_{xz-xz}| = 0.046$
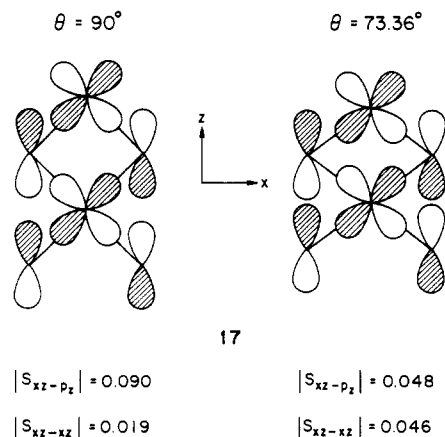
It is clear from the preceding argument that a considerable fraction of the shift in θ for both the contracted and expanded chains is due to P–P interaction. Just how much is shown in Figure 4. There are four curves of energy vs. θ. The two on the left are for the case of d^6, and the two on the right, for d^4. All curves are for the fragment within a solid, but curve

Table III. Overlap Population vs. θ

d^n		θ, deg 110	100	90	80	70
d^4	Fe–P	0.47	0.53	0.51	0.47	0.41
	$(P-P)_{\vec{z}}$	0.00	0.01	0.06	0.12	0.22
	$(Fe-Fe)_{\vec{z}}$	−0.03	0.00	0.03	0.07	0.09
	$(P-P)_{girth}$	0.24	0.00	−0.01	−0.01	0.00
d^6	Fe–P	0.50	0.53	0.52	0.47	0.37
	$(P-P)_{\vec{z}}$	0.01	0.00	0.00	0.00	0.05
	$(Fe-Fe)_{\vec{z}}$	−0.03	−0.06	−0.11	−0.17	−0.25
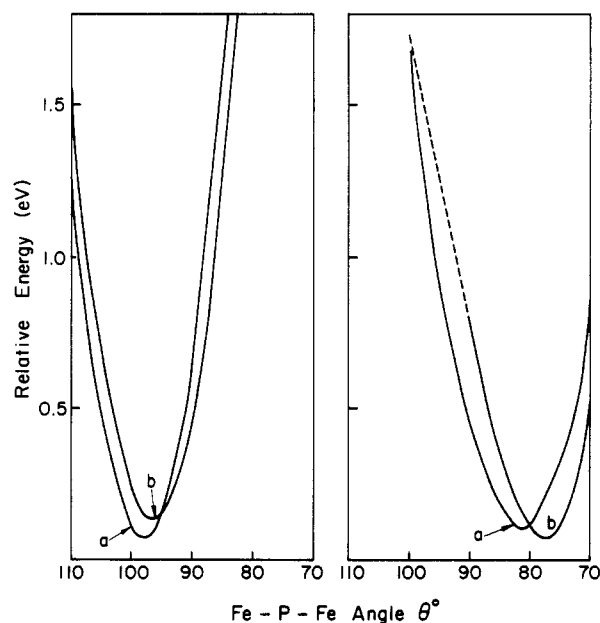
Figure 4. Relative energy curves for the fragment within a solid: d^6 on the left (two curves) and d^4 on the right (two curves). The dashed line refers to a discontinuity due to an avoided crossing; the notation a, b is explained in the text.

a has been calculated by subtracting the energies of the t_{2g} orbitals, thus giving a core effect.

Total energy curves can also be used to consider the appropriateness of the fragment within a solid approach. The two curves labeled b in Figure 4 should be compared to the d^4 and d^6 total energy curves for the infinite chain (Figure 5) and marcasite (Figure 1). The d^6 curves corresponding to filling all the t_{2g} as well as the core bonding orbitals are remarkably in agreement. Some disagreement (in θ_{min}) remains for the d^4 curves between the fragment and the chain, but not between the chain and marcasite. In fact, we shall later consider the nature of the d^4 conduction band (LUMO) at k
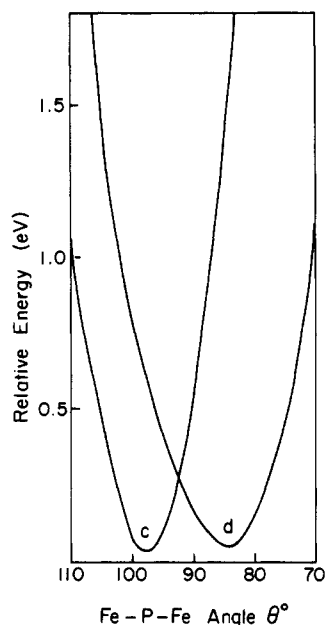
Figure 5. Relative energy curves for chains c (d^6) and d (d^4).

intermediate between the zone edge and center.

It is interesting to note that one aspect of these total energy curves can be compared to experiment. High-temperature studies show a thermal expansion of the unit cell along the chain axis for d^4, but only a minor effect for d^6.[12] According to our calculations (Figure 5d), the d^4 curve at the minimum is softer in the direction of high θ.

Other Chains: Rutile and NbCl$_4$

At this point we consider the effect of substituting other ligands. The experimental fact is that d^4 RuCl$_4$[13] is elongated, not contracted. We wish to examine this by substituting SH and Cl for PH$_2$. We included SH because (i) it is part of a continuum from PH$_2$ to Cl, (ii) it is an interesting potential ligand, and (iii) the local coordination around S is the same as S would have in the rutile structure (in fact, only O is found in the rutile structure).

Figure 6 indicates that for both SH and Cl a uniform contraction does not occur, θ_{min} being approximately 95 and 100°, respectively. The Walsh diagram indicates very clearly why this is so. The two orbitals emptied at the elongated geometry when we go from d^6 to d^4 are not σ^* and π^*, instead they are π and δ. Further, there is no emptying of σ^* and in particular p_z^* until the chain has contracted significantly. Hence, the d^4 chain feels the full repulsive force of the core and, for SH, the filled σ system.

There are two reasons why σ^* and p_z^* remain full. One is changes in the ligand p_z orbital as one goes across a period. In the sequence P, S, Cl, the elements get more electronegative, hence raising the distance p_z^* has to rise before it becomes unoccupied. Further, the p orbital contracts; this in fact reduces p–p overlap, which is the driving force for the rise of p_z^*.

A second factor, particularly important for SH, is the presence of high-lying M–M bonding orbitals δ and π. Something must be pushing these t_{2g} orbitals up in energy, and an obvious culprit is M–L π antibonding. The π interaction is considered in detail in the M$_2$L$_{10}$ paper,[1] and we will merely repeat those arguments we consider important. **16** shows why M–L interactions reverse the classical ordering $\pi < \pi^*, \delta <$

δ^*: π and δ have matches with ligand bridge orbitals whereas π^* and δ^* do not. But why does this reversal occur only for SH and Cl, not for PH$_2$? The ligand orbital involved in bonding to π and δ is p_y. In both SH and Cl this is a lone pair, but in PH$_2$ p_y is involved in P–H bonding, **18**. As a result
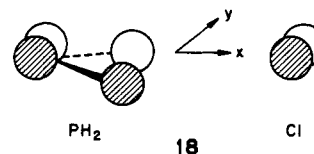
of P–H bonding, Fe–P interaction loses on two counts: the low-lying bonding orbital provides a poorer energy match, and the delocalized orbital, a poorer overlap. A related point of interest is that M–L π overlap is smaller for the case of Cl.

To get back to NbCl$_4$, we have shown that bridging Cl are not conducive to a contraction. Adding axial Cl adds more M–L π interaction. Since π and δ (and their antibonding components) are pushed up relative to σ and σ^*,[1] our previous argument still holds. Further, if we insist that the chain of axial Cl uniformly contracts, their repulsion would only increase the barrier to contraction.

A different picture is obtained if we substitute a ligand in row 2 of the periodic table. The major effect is that, in the range of distances corresponding to M–M bonding along the chain, there is virtually no contact between oxygen atoms. Hence, in our calculations on RuO$_2$ rutile, the only large changes on distortion are in Ru–Ru bonding. This is the reason the phenomenological model of Goodenough[14] for the electrical properties of rutile works extremely well.

Our calculations also give us information about the tendency of rutile to distort. We studied a uniform contraction of solid RuO$_2$ where the Ru–O distance was constant at 1.96 Å. The electron count was varied within a rigid-band model. For d^0 where we have an empty t_{2g} shell and for d^6 where both bonding and antibonding orbitals are filled, the minimum in energy was for an expanded chain. For other electron counts our calculations indicated that the chain would contract at least to a single Ru–Ru bond. Moreover, we measured the tendency to distort as the difference in energy between the chain at the experimental value of θ (Ru–Ru = 3.11 Å) and the chain where Ru–Ru = 2.65 Å, a single bond. This attractive energy decreased in the order $d^2, d^3 > d^1 > d^4 > d^5$.

Our results for d^4 and d^5 are in disagreement with experiment, due to the fact that our calculations leave out all repulsions that are not electronic in origin. On the other hand, the electron counts d^2, d^3, and d^1 are precisely those counts at which a pairing distortion is favored. We may not see the uniform contraction simply because the pairing distortion is even more energetically favorable.

## Band Structure and Electrical Properties

In this section we show that the unexpected semiconductivity of d^4 marcasite can be related to the bonding within the chain. In particular, it is necessary to have a band gap; the unoccupied (conduction) band is shown to be L–L antibonding at the zone center, M–M antibonding at the zone edge, and M–L antibonding halfway in between.

The section is organized as follows. First, we show that L–L bonding is a necessary precondition for a band gap. This is an interesting result in that it can be extended to other structures containing infinite trans-edge-sharing chains where the ligand is a four-coordinate pnictide. The compounds ReP$_3$ and TcP$_3$ have recently been synthesized by Rühl and Je-

(12) (a) Kjekshus, A.; Rakke, T. *Acta Chem. Scand., Ser. A* **1977**, *A31*, 517–529. (b) Kjekshus, A.; Rakke, T. *Ibid.* **1975**, *A29*, 443–452.
(13) Cotton, F. A.; Rice, C. E. *Inorg. Chem.* **1977**, *16*, 1865.

(14) Goodenough, J. B. In "Progress in Solid State Chemistry"; H. Reiss, Ed.; Pergamon Press: New York, 1971; Vol. 5, pp 145–399.
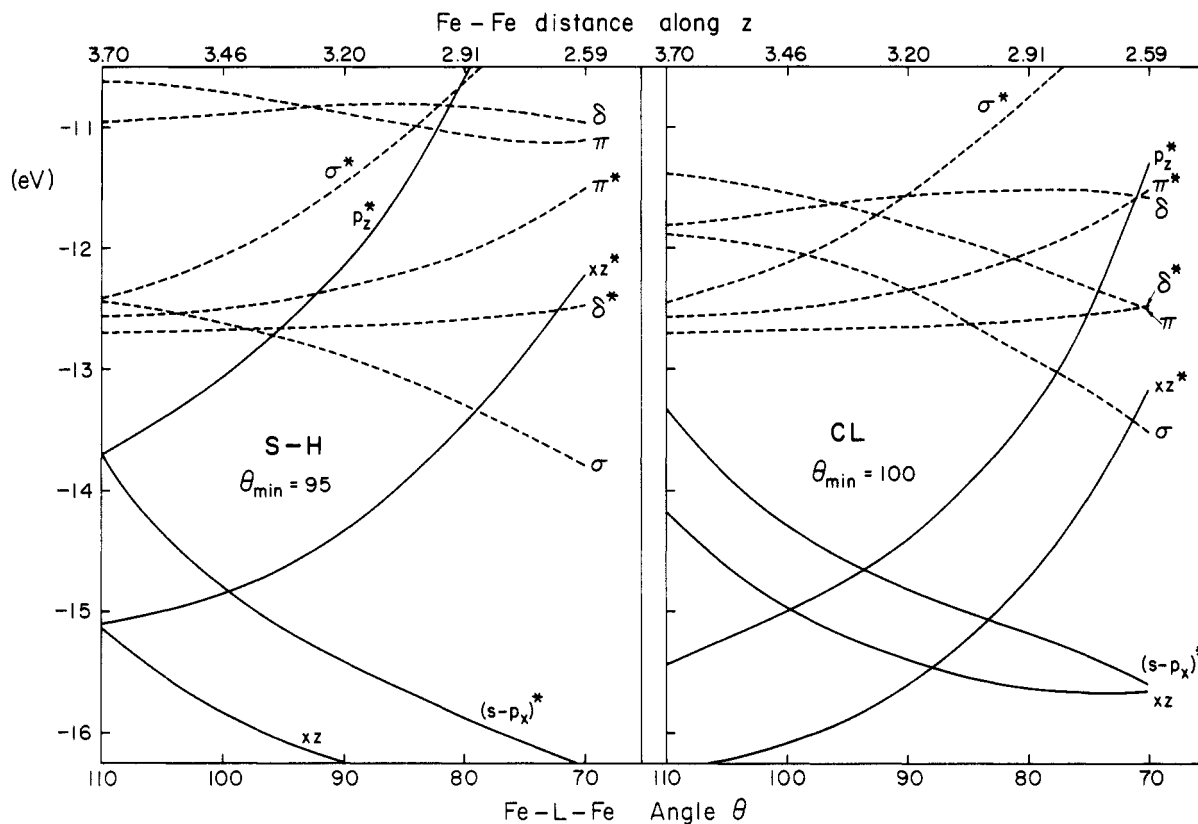
Figure 6. Walsh diagrams for the relevant orbitals of $[Fe(SH)_2H_2]_\infty$ and $[Fe(Cl)_2H_2]_\infty$. As before, the t_{2g} orbitals are represented by dashed lines and the core orbitals by solid lines. θ_{min} is the minimum in the total energy curve for the chain.

itschko.[15] If the electrical properties could be measured, we would have an experimental verification of P–P bonding along the chain axis (P–P = 3.09 Å). We shall derive this result using simple symmetry arguments and language such as "orbitals crossing one another" and "avoided crossing" that is familiar to chemists in another context: Walsh diagrams. Here we show that similar concepts can be used in constructing bands; however, they are very different physical objects.

Next, we show that the size of the band gap, which occurs between the zone center and zone edge, is determined largely by M–L interaction. We discuss the electrical properties of the model chains. Finally, we show that the band structure of three-dimensional marcasite is very similar to our model and discuss its electrical and magnetic properties in light of the experimental results.

Let us extrapolate from our "fragment within a solid", the orbitals at $k = 0$ and $k = 0.5$, to form bands. It is assumed that the reader understands how this process occurs for a chain of H atoms. For our chain, which contains more than one orbital per unit cell, we must ask the question "Which orbitals at $k = 0$ connect up with a particular orbital at $k = 0.5$?". One possibility is that the unit cell is essentially unchanged during this process: the only change is in translational symmetry. For instance, in Figure 7 ($\theta = 90°$), we see that $yz(\pi^*)$ connects to $yz(\pi)$ and $xy(\delta)$ connects with $xy(\delta^*)$. A second possibility is that the orbital changes character completely: this would go hand in hand with at least one avoided crossing whereas the previous possibility is consonant with only real crossings.

When do we get avoided crossings? When two orbitals have the same symmetry for those values of k at which the crossing could take place. This symmetry is not the rotational symmetry of the chain, D_{2h}, but a subset of symmetry operations
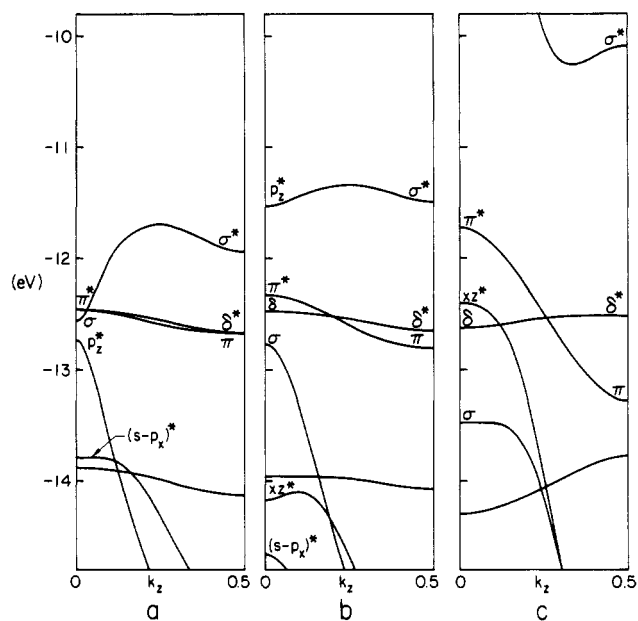
Figure 7. Band structures for three different geometries of the model chain, $[Fe(PH_2)_2H_2]_\infty$: a, $\theta = 97.5°$; b, $\theta = 90°$; c, $\theta = 73.36°$.

that take every atom into an equivalent *one in the same unit cell*. The reason for the last restriction[16] is that for a general k point there is no simple phase relationship (±1) between orbitals in different unit cells.

In our case the relevant symmetry is C_{2v} (principal axis z). Considering the t_{2g} orbitals, σ is a_1, π is b_2, and δ is a_2. Since π is antibonding at $k = 0$ whereas δ and σ are bonding at k

(15) Rühl, R.; Jeitschko, W. *Acta Crystallogr., Sect. B* **1982,** *B38,* 2784–2788.

(16) For a lucid discussion of this point see: Tinkham, M. "Group Theory and Quantum Mechanics"; McGraw-Hill: New York, 1964; pp 281–284.
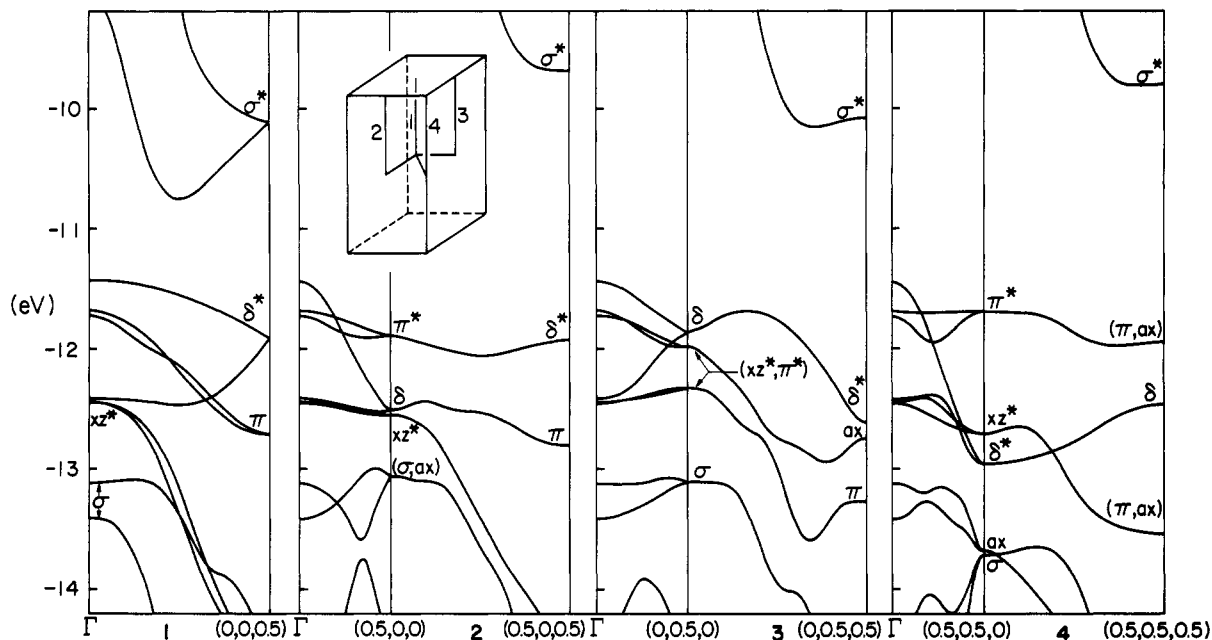
Figure 8. Band structure of FeP_2 marcasite along the symmetry lines indicated in an inset.

= 0, these orbitals cross one another in k space (Figure 7, θ = 97.5°). Hence, if these were the only high-lying orbitals, the d^4 chain would be a metal. However the high-lying orbital, p_z^*, at $k = 0$ has a great dispersion (14) and symmetry a_1. Hence, it undergoes an avoided crossing with the σ band.

The avoided crossing is easily seen in Figure 7 ($\theta = 90°$). The orbital that starts out as σ becomes the quickly falling core orbital whereas the upper p_z^* orbital does not change much in energy as its character changes to σ^*.

The important point is that a gap is opened up between d^4 and d^6. The size of the gap, which is also pertinent to the electrical properties of marcasite, is controlled by the *strength* of the avoided crossing. This involves d_σ–p_z overlap and is *M–L antibonding.*[17]

How important is M–L antibonding? To find out, we turn off M–L interaction at $k = 0.25$, halfway between the zone center and zone edge. Since the phase factor between the same orbital on nearest-neighbor unit cells is $e^{i\pi/2}$, there is no through-space $d_{z^2-x^2}$–$d_{z^2-x^2}$ bonding. Hence, all metal orbitals are approximately degenerate; a small splitting is caused by metal d–p hybridization. On the other hand, turning on M–L interaction leads to a band gap at $k = 0.25$ of 1.2 eV at $\theta = 90°$.

When $[Fe(PH_2)_2H_2]_\infty$ is contracted, the whole conduction band moves up in energy (Figure 7). We know why this happens at $k = 0$ and $k = 0.5$. At $k = 0.25$ the LUMO moves up due to an increase in the relevant M–L overlap integral, between metal d_{z^2} and phosphorus p_z. On the other hand, the valence bands, d_{yz} and d_{xy}, do not move up in energy; they just broaden. At the contracted geometry, the indirect (electrical) band gap from $\pi^*(0)$ to the LUMO at $k \sim 1/3$ is $1 1/3$ eV, the direct (optical) gap much larger.

Three-Dimensional Marcasite

Figure 8 depicts the band structure of FeP_2 marcasite along symmetry lines indicated in an inset. This band structure can be correlated to electrical and magnetic properties, Table II. The indirect band gap for FeP_2 is 0.75 eV; a gap of about that

size occurs along the line $\Gamma \rightarrow$ (0, 0, 0.5). In contrast, the experimental value is 0.4 eV. In contrast to the model chain the direct (optical) gap is not much larger than the indirect gap.

Table II shows that the only known electron count $<d^4$ for binary marcasites is d^2, for which the structure is uniformly contracted, and the ground state is either paramagnetic or antiferromagnetic, depending on the temperature. The filling d^2 is marked on the DOS curves for both the solid and the chain (dashed lines in Figures 9 and 10). In the *solid*, the Fermi level lies in a region of relatively high density of states and between two large peaks. A solid with a large number of states near the Fermi level is similar to a small-gap molecule: it is likely that the narrow bands will split to relieve Coulombic repulsion, perhaps resulting in a magnetic ground state, perhaps in a charge density wave.[18] It is unlikely that the d^2 *chain*, in which the Fermi level is close to the very sharp δ peak, would be a metal.

It is clear from our discussion of its structure that marcasite is not quasi-one-dimensional. Yet, our calculations indicate that trends in the total energy and overlap populations for the solid as a function of θ are in complete agreement with those for the model chain. Moreover, it is possible to examine these trends as a function of the set of k points averaged over in the solid: results for a special points set chosen to emphasize dispersion along the chain axis are in complete agreement with those for a more isotropic set. The rest of this section will be devoted to showing why the one-dimensional model works so well.

We first compare the four lines involving dispersion along z in Figure 8 with the band structure of the contracted chain, Figure 7c. We must first do some counting: since there are two ML_2 units per unit cell, there are twice as many metal or phosphorus bands along the line $\Gamma \rightarrow$ (0, 0, 0.5) as there are in the chain. Along the other three lines k_x and/or k_y = $1/2$ and at the point $k_z = 1/2$, there are as many metal or phosphorus bands as in the chain: each band is doubly degenerate since the unit cell contains two chemically equivalent units related by a screw axis.

We are now ready to compare marcasite to the chain. The strong P–P interaction is indicated in the two (four) bands,

---

(17) This is consistent with the experimental fact that as we go down a group of ligands (i.e. replace P by As or Sb) the size of the electrical gap remains fairly constant. L–L interactions increase, and M–M interactions decrease (Figure 11) so the size of the band gap must be controlled by M–L interaction.

(18) Whangbo, M.-H. *Acc. Chem. Res.* **1983**, *16*, 95.
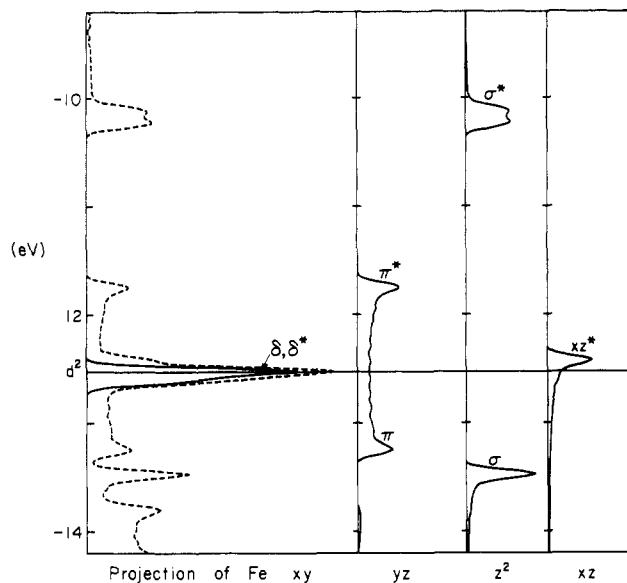
Figure 9. Projections of the high-lying orbitals of the contracted model chain. The dashed curve refers to the total DOS, and the solid curves refer to the projections.
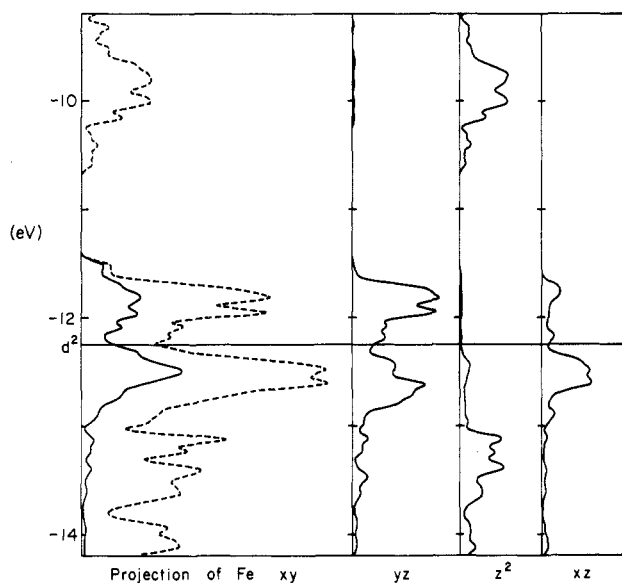

Figure 10. Projections of the high-lying orbitals of FeP_2 marcasite. The dashed curve refers to the total DOS, and the solid curves refer to the projections.

which fall rapidly with changing k_z, for all four examples in Figure 8. Evidence for the avoided crossing in the figure is the gap above the count d^4, σ^* correlating to a very high orbital and σ turning into a rapidly falling band. We also note that π^* is usually higher than π.

Orbital projections as well as the total density of states are shown for marcasite in Figure 10, and the comparable diagram for the chain is shown in Figure 9. The vertical energy scale allows one to make the connection between these figures and MO diagrams; each baseline corresponds to a different metal basis orbital, hence π and π^*, σ and σ^*, or δ and δ^* are in the same projection. Figure 9 is beautiful in its simplicity: because the derivative of a band is zero[19] at the zone center and zone edge, there is a peak for each of the "fragment within a solid" orbitals. The narrow δ band gives only a single sharp peak.
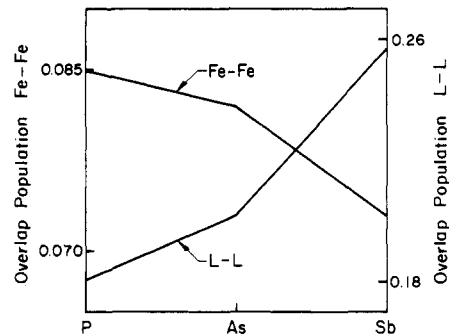
Figure 11. Overlap population for the model chain in which the equatorial ligand is successively PH_2, AsH_2, and SbH_2. The different scales used for Fe–Fe and L–L overlap population are not an indication that L–L bonding is stronger than Fe–Fe bonding.

The projection π is that of a textbook "cosine" band whereas the break between σ and σ^* is indicative of an avoided crossing. The second (lower) peak in σ^* is due to the minimum, at intermediate k, in the conduction band.

Clearly, dispersion perpendicular to the chain axes in marcasite has made Figure 10 more complicated. For instance, note the broadening of what was a narrow δ band. Fundamentally, however, Figure 10 is remarkably similar to Figure 9. In particular, note the roughly classical order of metal t_{2g} orbitals (σ lowest, σ^* highest) and the high-lying xz projection, which is symptomatic of reduced Fe–P bonding.

Comparison with Experiment

To quote a previous author,[20] "compounds with the FeS_2 marcasite type crystal structure have been subjected to regular investigations throughout most of this century". One result of this extensive study has been a great variety of marcasites found, structural data as well as electrical and magnetic properties for which have been summarized as a function of electron count in Table II[21] (we have not included counts greater than d^6).

To what extent is the structural data in accord with our band calculations? Our most important conclusion was that the ligands could not be neglected. This is a consequence of the fact that the shortest M–M distances along z are the same as the shortest L–L distances along z. Hence, in FeP_2 when the Fe–Fe distance shortened to 2.7 Å, the resulting P–P distance, although 0.4 Å greater than a single bond, was clearly a contact.

Even more convincing evidence for the role of the ligands comes from examining the series FeP_2–$FeAs_2$–$FeSb_2$. We see that θ is remarkably constant: hence θ is a very good parameter to measure contraction as has been noted elsewhere. However look what this constancy of θ implies for the shortest contact along z: 2.7 Å in FeP_2 increasing to 3.2 Å in $FeAs_2$, in one case a distance characteristic of an Fe–Fe single bond and in the other case no Fe–Fe bond.

Does this imply, as has been suggested by others,[21c,22] that there is no Fe–Fe bond in this class of compounds? Certainly the Fe–Fe overlap population in FeP_2 would suggest otherwise. However, it does indicate that the ligands must also be important, and corresponding to increasing Fe–Fe distance there is a reduction in the difference between the contact L–L

(19) Our density of states calculated from a histogram over a finite number of points in k space does not show the singularities inherent in an ideal one-dimensional system.

(20) Kjekshus, A.; Rakke, T. *Acta Chem. Scand., Ser. A* **1974**, *A28*, 1001–1010.

(21) (a) Holseth, H.; Kjekshus, A. *Acta Chem. Scand.* **1968**, *22*, 3284–3292. (b) Kjekshus, A.; Rakke, T.; Andresen, A. F. *Acta Chem. Scand., Ser. A* **1974**, *A28*, 996–1000. (c) Kjekshus, A.; Rakke, T.; Andresen, A. F. *Ibid.* **1977**, *A31*, 253–259. (d) Brostigan, G.; Kjekshus, A. *Acta Chem. Scand.* **1970**, *24*, 2993–3012.

(22) Goodenough, J. B. *J. Solid State Chem.* **1972**, *5*, 144–152.

distance and the closer L–L distance corresponding to a single bond. Presumably this implies that a loss in metal bonding is compensated by an increase in ligand bonding. Figure 11 shows that the trend in overlap populations is the expected one.[23]

The most intriguing of the previous, qualitative, attempts to explain marcasite is due to Goodenough.[22] Goodenough realized that there must be a mechanism to lift a single band above all others (within the d^6-occupied manifold), and he suggested that this mechanism was M–L antibonding. If strong enough, this could unoccupy the complete d_{z^2} band including its most M–M bonding part. In contrast, we find that d_{z^2} is involved in strong M–L interaction only in part of the Brillouin zone; hence, this mechanism is not sufficient to account for the band gap.

Recently, Tossell[24] et al. developed an alternate theory that also cites M–L interaction as the cause of the band gap. Crucial to their theory is L–L bonding in the L_2 units of three-dimensional marcasite (as opposed to the longer L–L distance along the chain). Accordingly only P_2 π^* orbitals are important for the band gap; the gap is due to the local geometry around P in contracted marcasite, causing one of the P_2 π^* orbitals to be involved in stronger M–L interaction than the other.

Our calculations do not support the hypothesis that of the P_2 orbitals only π^* are important for the band gap: we find that the ligand p_z contribution to the conduction band of marcasite consists of approximately equal contributions from P_2 π^* and P_2 π. Further, the experimental evidence is that the L–L bond length does not increase as the electron count varies from d^4 to d^6, for example in the series $FeAs_2$, $CoAs_2$, $NiAs_2$. L–L distances in Table II are characteristic of a single bond.

An implication of both Goodenough's and Tossell's arguments is that the contraction of d^4 marcasite is due to M–L bonding (the unoccupied orbital is increasingly antibonding). In contrast, we find that equatorial bonding decreases as θ increases: Goodenough did not consider the contribution from the core. There is experimental evidence, not conclusive, that indicates we are correct. First, if we compare the two non-equivalent distances (M–L) axial and (M–L) equatorial in the solid,[25] the latter is always larger than the former (Table II). Hence, equatorial bonds are weaker than axial bonds, a fact with which our overlap populations agree. However, this evidence is inconclusive in answering the question of whether equatorial bonds get stronger or weaker on contraction (comparing d^6 to d^4 marcasites).

A second piece of evidence comes from Mössbauer and structural studies on $FeSb_2$ and $FeAs_2$ into which nickel has been doped.[20] We may consider Ni to be an electron source; the chain $d^{4+\Delta}$ expands along z as the amount of nickel increases, and there is a trend toward (1) a smaller δ, the ^{57}Fe Mössbauer chemical shift parameter (This is consistent with a smaller occupation of d orbitals, which could occur as the almost M–L nonbonding xz^* orbital (mostly d on metal) becomes increasingly M–L bonding (roughly equal metal d and ligand p). Similarly, Mössbauer chemical shifts for d^6 FeS_2 are the same as for d^4 $FeAs_2$,[26] despite the fact that the d^4 conduction band is partly metal.) and (2) a smaller average M–L bond length.
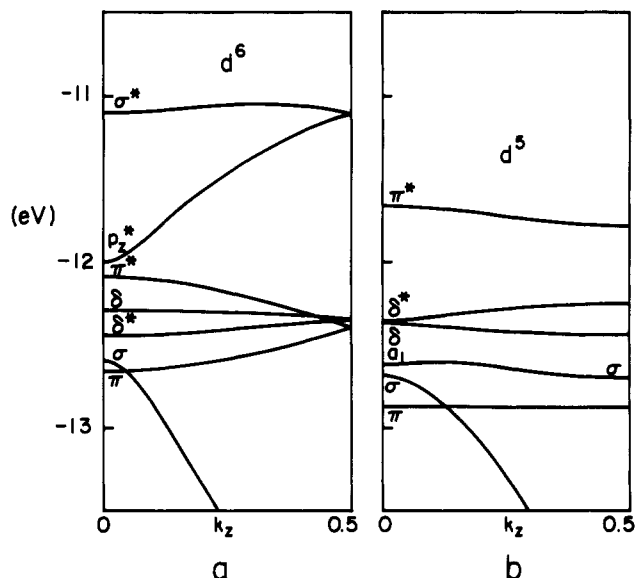

Figure 12. Band structures for two different geometries of the model Rh chain, $[Rh(PH_2)_2H_2]_\infty$: a, $\theta_1 = \theta_2 = 90°$; b (the paired chain), $\theta_1 = 70.6°$, $\theta_2 = 102°$. The orbitals labeled p_z^* and σ^* in a mix in b. The positive combination is labeled a_1, whereas the negative combination is off scale, at about –8 eV.

Nonuniform Contraction

Historically the solid resulting from the pairing distortion of d^5 marcasites has been given the name arsenopyrite. The change in name reflects the fact that the symmetry of arsenopyrite, which is monoclinic C_{2h}^5, is lower than the symmetry of marcasite. With the metal as origin, there are no point operations in arsenopyrite; there is however an inversion center halfway between two metal atoms.

Structures of the arsenopyrites have been determined for most group 5A ligands.[27] These studies indicate that, other than pairing along the chain axis, there are only minor changes that involve the movement of the chains relative to one another. As before we use the angle θ at the bridging ligand to describe the distortion within a chain; now we need two values of θ, θ_1 for the contracting ML_2M quadrilateral and θ_2 for the expanding ML_2M quadrilateral, as shown in **6**.

We now describe some structural details of pairing in model chains, which are similar to **13** but where Fe has been replaced by Rh. The contraction has been idealized by choosing all M–L distances equal and keeping the metal–equatorial ligand–metal–equatorial ligand backbone planar. The chains are contracted from uniform ($\theta_1 = \theta_2 = 90°$) to experimental geometry, as defined by the values of θ in Table II for RhP_2 and $RhSb_2$.

The most important feature of the pairing distortion is that the ligand backbone remains uniformly spaced along z; only the metals need move. Hence, L–L repulsion need not increase, in marked contrast to what happens during a uniform contraction, a fact which has prompted others[2] to refer to pairing in $NbCl_4$ as a low-energy transit. In our case, with P as the bridging ligand, there is some contraction of the P–P distance along z, from 3.34 Å (90°, 90°) to 3.23 Å (final geometry).

Of greater importance is bumping of ligands along the x axis. Such bumping occurs in the expanding link of the chain; hence, the deviation of θ_2 from 90° is less than the corresponding deviation of θ_1. This effect is particularly marked for $RhSb_2$: the large Sb ligands allow a value of only 93° for

(23) It is, of course, dangerous to compare P–P overlap populations with Sb–Sb overlap populations. Nevertheless, an extended Hückel calculation on P_4, As_4, and Sb_4 at the "single-bond" distance in marcasite gave overlap populations within 0.01 of one another.

(24) Tossell, J. A.; Vaughan, D. J.; Burdett, J. K. *Phys. Chem. Miner.* **1981**, *7*, 177–184.

(25) With the exception of the magnetic compound d^2 $CrSb_2$.

(26) Vaughan, D. J.; Craig, J. R. "Mineral Chemistry of Metal Sulfides"; Cambridge University Press: Cambridge.

(27) (a) Kjekshus, A. *Acta Chem. Scand.* **1971**, *25*, 411–422. (b) Zdanov, G. S.; Kuz'min, R. N. *Sov. Phys.—Crystallogr. (Engl. Transl.)* **1961**, *6*, 704–711.
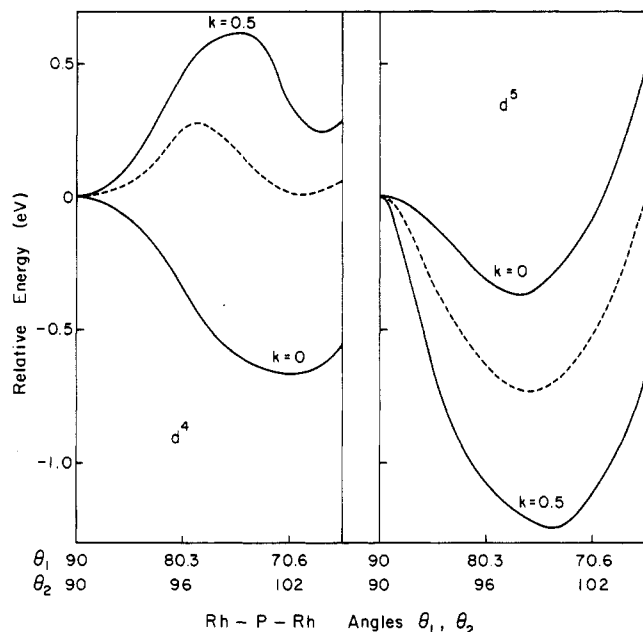
Figure 13. Relative energy curves for the pairing distortion of the Rh chain. The total energy curves shown are those of the chain (dashed lines) and its $k = 0$ and $k = 0.5$ orbital subsets (solid lines). Note the common zero at the uniform geometry.

θ_2. Nevertheless, it remains true that if we could draw a d^0 curve for this process (low symmetry makes this difficult), it would be much shallower than for the uniform contraction.

The difference between the uniform backbone of phosphorus and the nonuniform backbone of metals is clearly seen in the band structure of the model chain (Figure 12). In Figure 12a, $\theta_1 = \theta_2 = 90°$, we have doubled the unit cell in anticipation of a pairing distortion. Doubling the unit cell in real space is equivalent to halving the reciprocal space Brillouin zone so that Figure 12a is similar to Figure 7 except that the zone edge in the former is $k = 0.25$ and the bands have been folded back on themselves (in particular the electron counting is the same as in Figure 7). Figure 12b shows the band structure at the experimental value of θ. The pairing distortion has split the metal "t_{2g}" bands so that, instead of a single wide band per t_{2g} orbital, there are two narrow bands, one bonding and one antibonding, with a gap between. The narrow bands are indicative of a localization of the orbitals. In contrast, p_z^*, the orbital mainly derived from phosphorus, has a considerable bandwidth. This bandwidth is somewhat obscured by an avoided crossing with the σ band. Finally, note the band gap for the d^5 contracted chain, in agreement with its semiconducting properties.

According to experiment the count d^4 leads to a uniform contraction, and the count d^5 to a pairing distortion. We now examine this point theoretically, starting with the uniform chain $\theta = 90°$. Figure 13 shows the total energy for the pairing distortion of the chain $[Rh(PH_2)_2H_2]_\infty$ corresponding to a linear transit in θ_1 and θ_2 between the uniform chain and the experimental values already defined. We might worry about the substitution of Rh for Fe, but in fact calculations show that it makes no difference to the relative energy curves, Figures 2 and 5, corresponding to the uniform contraction. The energy scales are not identical since one unit cell for the paired chain is equal to two unit cells for the uniform chain. We will quote the values for the larger unit cell. The d^5 chain gains 17 kcal mol^{-1} per unit cell from the pairing distortion but is at the minimum of the uniform contraction. The d^4 chain gains 5 kcal mol^{-1} per unit cell from the uniform contraction; we believe that this value is low since the final value of θ is too high. For this electron count there is a barrier to

pairing. Finally, our calculations for electron counts d^0–d^3 show that the uniform contraction is allowed and the pairing distortion not allowed.

**Energy and Bonding: Comparison to Other Ligands**

In the concluding section of the paper, we will trace the reason pairing occurs preferentially for d^5 rather than d^4 or lower electron counts. By tracing the impetus for pairing to a single orbital, we will be able to extend our results to other ligands (the known experimental results are summarized in Table I). A general rule relating pairing to the nature of the ligand is important for the following reason. Experimentalists are interested in producing metallic conductors, especially one-dimensional conductors. A pairing distortion that leads to either semiconductivity or weak metallic behavior (note the narrow bands in Figure 12b) is something to be avoided. This point has been examined in great detail by Shaik et al. for NbCl$_4$.[2c]

In addition to depicting the average total energy curves for the chain, Figure 13 contains total energy curves for the values of k corresponding to the zone center and zone edge. Both zone center curves favor pairing; the zone edge curves have the same shape as the average total energy. Hence, the reason pairing occurs preferentially for d^5 is to be found at the zone edge.

To the reader familiar with Peierls distortions, the fact that the principal driving force for the distortion is at the zone edge will come as no surprise. Let us first consider the effects of M–M bonding, which has been shown to be the driving force in NbCl$_4$. Clearly σ bonding is the first to be turned on. Looking at the σ type orbitals in Figure 12, we see that the $k = 0.5$ orbital has to drop quite a bit in energy but the $k = 0$ orbital hardly changes. A simple bonding argument explains this result. At the zone edge, one d_σ orbital gains σ bonding (contracted link) and loses σ antibonding (expanded link); the other d_σ orbital gains σ antibonding and loses σ bonding. In contrast, at the zone center one orbital gains and loses σ bonding; the other gains and loses σ antibonding.

19 shows the orbitals derived from d_σ at the paired geometry.

19
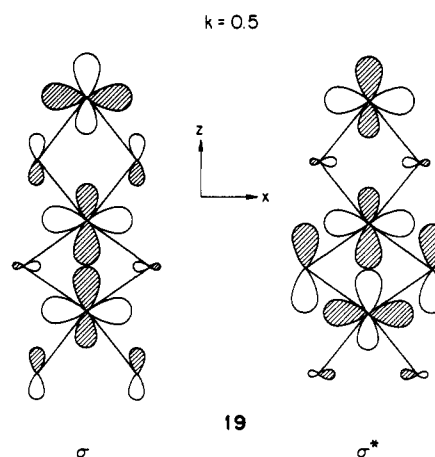
It depicts the differential effects of M–M bonding referred to in the previous paragraph (we shall use d_σ to refer to the $k = 0.5$ orbitals of the unpaired geometry but σ and σ^* to refer to its derivatives in the paired geometry).

However, unlike in NbCl$_4$ there is also a strong effect due to the ligands: this fact should come as no surprise since the orbital of the unpaired chain is substantially M–L π antibonding. In our earlier discussion, we showed that the extent to which ligand p_z participates in π antibonding increases as the chain contracts: this caused an increase in the gap at $k = 0.25$ in the unpaired chain. It also adds to the driving force for the pairing distortion: in σ^* the phosphorus p_z orbital is in the contracted link (more destabilization), and in σ the
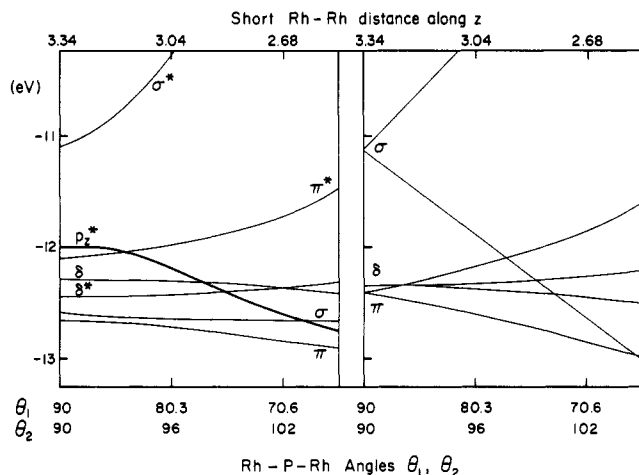
Figure 14. Walsh diagram for the pairing distortion of the Rh chain containing the orbitals at (left) $k = 0$ and (right) $k = 0.5$. Core orbitals are drawn with a thicker line.

phosphorus p_z orbital is in the expanded link. The relative sizes of these ligand orbitals in **19** are drawn to scale.

Figure 14 is the Walsh diagram for $k = 0$ and $k = 0.5$. It shows us what we already suspected: the most dramatically falling orbital is σ at $k = 0.5$. Due to M–L π antibonding, this orbital is very high in energy at the starting geometry. Hence, it *remains the d^5 HOMO* along three-fourths of the transit to experimental geometry. For d^4, both σ and σ^* ($k = 0.5$) are unoccupied during this part of the transit and, rather than bonding, we have filled-shell repulsion. This accounts for the barrier to pairing. For electron counts less than d^4, σ is occupied even later along the transit.

It is also interesting to examine the "a_1" manifold at $k = 0$. The orbitals shown in **20** are derived from p_z^* and σ^* in

$$k = 0$$
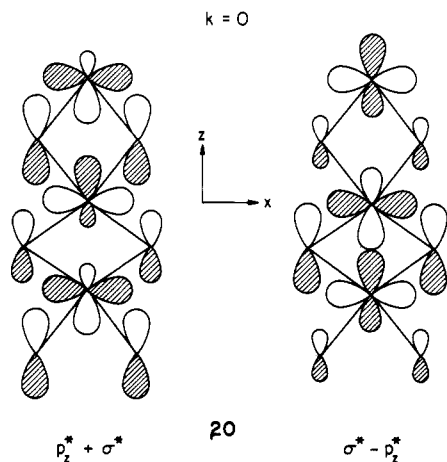
the uniform chain, but the lowering of symmetry has allowed them to mix. The important point is that the upper orbital, σ^*–p_z^*, which is unoccupied, contains both M–M and P–P antibonding components. Hence, like d^4 marcasites, d^5 arsenopyrites contain P–P as well as M–M bonding. If Sb replaces P in the chain, L–L overlap population increases but M–M overlap population decreases, analogous to Figure 8. L–L bonding is needed to explain the long (longer than single bond) Rh–Rh contact in RhSb$_2$.

We have just shown that we can predict the electron count at which arsenopyrite undergoes a pairing distortion by knowing the level of the d_σ orbital at $k = 0.5$ for the *unpaired* chain. For distortion to occur d_σ must not be too far above the Fermi level. On the other hand, if d_σ were far below the Fermi level, σ^* would remain occupied during most of the transit; since σ^* is a rapidly rising orbital, pairing would not occur. In short, pairing is most likely to occur for those
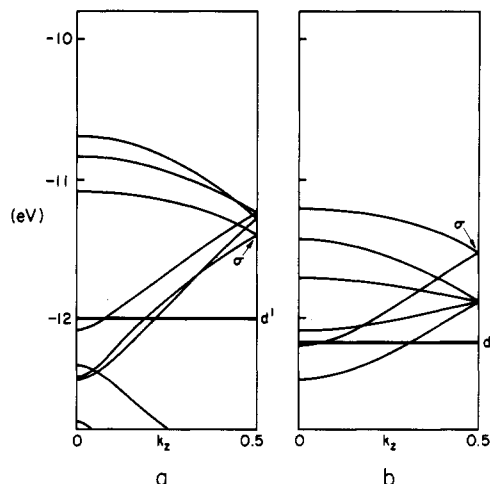
Figure 15. Band structure for the uniform geometry ($\theta_1 = \theta_2 = 90°$) for the model chains $[\mathrm{Rh(SH)_2H_2}]_\infty$ and $[\mathrm{Rh(Cl)_2H_2}]_\infty$ showing the relative positions of the Fermi level for electron count d^1 and the energy of the orbital σ ($k = 0.5$).

Table IV. Extended Hückel Parameters

orbital	H_{ii}	exponents	orbital	H_{ii}	exponents
Fe 3d	−12.7	5.35 (0.5366)	P 3s	−18.6	1.88
		1.80 (0.6678)	3p	−14.0	1.63
4s	−9.17	1.90	As 4s	−18.6	2.23
4p	−5.37	1.90	4p	−14.0	1.89
Rh 4d	−12.5	4.29 (0.5807)	Sb 5s	−18.6	2.32
		1.97 (0.5685)	5p	−14.0	2.00
5s	−8.09	2.13	S 3s	−20.0	2.12
5p	−4.57	2.10	3p	−13.3	1.83
H 1s	−13.6	1.30	Cl 3s	−30.0	2.36
			3p	−15.0	2.04

electron counts for which the Fermi level is close in energy to d_σ.

How could we change ligands in our model chain, or in arsenopyrite, to cause pairing to occur at electron counts other than d^5? One strategy is to push down the orbital d_σ; the other strategy is to push up some of the other orbitals. Reducing M–L π antibonding by choosing a ligand to the right of phosphorus or one in row 2 of the periodic table accomplishes the first goal. The second goal can be accomplished by replacing bridging and/or axial ligands PH$_2$ and H by π donors. According to our previous discussion, such a perturbation can only push up d_π and d_δ orbitals, never d_σ, **16**.

Figure 15 shows the band structure for the model chain in which only equatorial ligands have been substituted. In accord with the previous paragraph, d_σ has moved down in energy and parts of the π and δ d bands have moved up in energy. Our model would predict that pairing occurs for lower electron counts. Total energy curves were calculated for these two cases with the assumption that θ_1 and θ_2 were varied in the same ratio to one another as in the case of bridging PH$_2$. The minimum in energy was at a paired geometry for the electron counts d^2–d^4 (SH) and d^2–d^5 (Cl).

In the experimental structures *NbCl$_4$* and *rutile*, the axial ligand has also been substituted by a π donor. Our model would predict pairing at even lower electron counts, which is exactly what the experimental data (Table I) show. An axial ligand that was an acceptor would have the opposite effect. This is in accord with the theoretical results of Shaik[2c] that, for the trimer Nb$_3$Cl$_8$(CO)$_6$, pairing occurs only for the electron count d^5. Our simple model works; and it would be interesting to determine its limits by an experimental test.

Acknowledgment.

greatly to the computer programming that made this project possible. Our research was generously supported by National Science Foundation Grant DMR 7681083 to the Materials Science Center at Cornell University.

Appendix I

Extended Hückel parameters for all atoms used appear in Table IV. Ligand and metal H_{ii} and metal exponents are from previous work,[28] except that As and Sb H_{ii} are set equal to P H_{ii}. Ligand exponents are from Clementi and Roetti.[29]

For L = P, S, and Cl, Fe–L = 2.26 Å and Rh–L = 2.36 Å. Other Fe–L distances were 2.38 (As) and 2.60 Å (Sb). L–H distances were 1.43 (P), 1.33 (S), 1.52 (As), and 1.78

Å (Sb). All M–H distances were 1.57 Å. P–P = 2.24 Å in three-dimensional marcasite.

All these distances were kept constant during distortion; only the angle θ was varied. Special values of θ were 73.36 (uniform contraction), 97.5 (uniform expansion), 70.56 (θ_1), and 101.96° (θ_2) for the pairing distortion.

Appendix II

A special points set is a set of k points of size n, designed to give the best value for average properties of the solid for a given n. Our sets were adapted from a standard reference;[10b] the optimal size n was obtained by comparing sets of different size. For one-dimensional problems we used the three-point set $\{(^1/_{12}, ^3/_{12}, ^5/_{12})\}$. A three-point anisotropic set $\{(^1/_4, ^1/_4, k_z)\}$ $k_z = ^1/_{12}, ^3/_{12}, ^5/_{12}\}$ and a twelve-point more isotropic set $\{(^1/_8, ^1/_8, k_z), (^1/_8, ^3/_8, k_z), (^3/_8, ^1/_8, k_z), (^3/_8, ^3/_8, k_z)$ $k_z = ^1/_{12}, ^3/_{12}, ^5/_{12}\}$ were used for orthorhombic marcasite.

(28) (a) Summerville, R. H.; Hoffmann, R. *J. Am. Chem. Soc.* **1976**, *98*, 7240–7254. (b) Schilling, B. E. R.; Hoffmann, R. *Ibid.* **1979**, *101*, 3456–3467.
(29) Clementi, E.; Roetti, C. *At. Data Nucl. Data Tables* **1974**, *14*, 179–478.

Contribution from the Department of Chemistry,
University of Utah, Salt Lake City, Utah 84112

# Reaction of Tetraborane(10) with Trimethylphosphine in Tetrahydrofuran

MAMORU SHIMOI and GOJI KODAMA*

When tetraborane(10) was treated with trimethylphosphine in a 1:1 molar ratio in tetrahydrofuran at −90 to −70 °C, $(CH_3)_3P\cdot BH_3$, $THF\cdot B_3H_7$, and $H_2B(THF)_2{}^+B_3H_8{}^-$ were produced. The formation of $(CH_3)_3P\cdot B_3H_7$ was minimal. The same reaction was performed in dimethyl ether, diethyl ether, and dichloromethane, and the patterns of product distribution were compared with each other. The previously proposed mechanism for the B_4H_{10} cleavage reactions was used to explain the observed results by taking the effects of concentrations and strength of the reacting bases into consideration. This mechanistic model explained also the results of the reactions of B_4H_{10} with trimethylamine and phosphine in tetrahydrofuran. The values of 4 ± 1 and 0.41 ± 0.02 were obtained as the equilibrium constants for $(CH_3)_3P\cdot BH_3 + THF\cdot B_3H_7 \rightleftharpoons THF\cdot BH_3 + (CH_3)_3P\cdot B_3H_7$ at 25 °C and $H_3P\cdot BH_3 + THF\cdot B_3H_7 \rightleftharpoons THF\cdot BH_3 + H_3P\cdot B_3H_7$ at 0 °C, respectively.

Introduction

The cleavage reactions of tetraborane(10) B_4H_{10} with Lewis bases have been classified into two categories:[1] symmetrical cleavage

$$B_4H_{10} + 2L \rightarrow L\cdot BH_3 + L\cdot B_3H_7$$
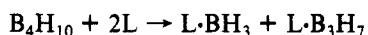
and unsymmetrical cleavage

$$B_4H_{10} + 2L' \rightarrow H_2BL'_2{}^+ + B_3H_8{}^-$$
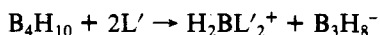
where L and L′ represent Lewis bases. Many examples of these reactions have appeared in the literature.[2] However, the cases in which B_4H_{10} are reacting with two different bases, such as "B_4H_{10} + L(1) + L(2)", have not been reported.

Recently, we described the reaction of B_4H_{10} with trimethylphosphine *in tetrahydrofuran* as an observation in connection with the characterization of a new anion B_4H_9P-$(CH_3)_3{}^-$.[3] The products in the reaction were "$(CH_3)_3P\cdot BH_3$ **and** $THF\cdot B_3H_7$", and were **not** "$(CH_3)_3P\cdot B_3H_7$ **and** $THF\cdot BH_3$". The latter pair of adducts would be the products that one would normally expect on the basis of the acid–base strength of the species involved. This finding prompted us to investigate

the reaction in more detail in efforts to find the factors that determine the "anomalous" product formation.

Results and Discussion

A. Reactions of Trimethylphosphine with $H_2B(THF)_2{}^+B_3H_8{}^-$ and with "$THF\cdot BH_3 + THF\cdot B_3H_7$". Trimethylphosphine, $P(CH_3)_3$, is a much stronger base than tetrahydrofuran,[4] and therefore the rate and extent of reaction of tetraborane(10) with trimethylphosphine are expected to be greater than those with tetrahydrofuran. However, when the reaction of tetraborane(10) with trimethylphosphine is performed in tetrahydrofuran as the solvent, due to the predominant concentration of tetrahydrofuran in the reaction mixture, B_4H_{10} will react with both $P(CH_3)_3$ and tetrahydrofuran, and the products of the tetrahydrofuran reaction will further react with $P(CH_3)_3$. The reactions of the B_4H_{10}–tetrahydrofuran reaction products with $P(CH_3)_3$, therefore, were investigated first.

Earlier, Schaeffer, Tebbe, and Phillips[5] found that B_4H_{10} reacted with tetrahydrofuran at −68 to −53 °C to form H_2B-$(THF)_2{}^+B_3H_8{}^-$, which at higher temperatures (above −24 °C) changed into a 1:1 mixture of $THF\cdot BH_3$ and $THF\cdot B_3H_7$. We reinvestigated the reactions using a larger quantity of tetrahydrofuran than that in the earlier study and found that the formation of $H_2B(THF)_2{}^+B_3H_8{}^-$ slowly proceeded to completion even at −80 °C.

(1) (a) Edwards, L. J.; Hough, W. V.; Ford, M. D. *Proc. Int. Congr. Appl. Chem.* **1958**, *16*, 475. (b) Kodama, G.; Parry, R. W. *Ibid.* **1958**, *16*, 483. (c) Parry, R. W.; Edward, L. J. *J. Am. Chem. Soc.* **1959**, *81*, 3554.
(2) (a) See, for example: Shore, S. G. In "Boron Hydride Chemistry"; Muetterties, E. L., Ed.; Academic Press: New York, 1975; Chapter 3. (b) Dodds, A. R.; Kodama, G. *Inorg. Chem.* **1977**, *16*, 3353.
(3) Shimoi, M.; Kodama, G. *Inorg. Chem.* **1983**, *22*, 1542.
(4) Coyle, T. D.; Stone, F. G. A. In "Progress in Boron Chemistry"; Steinberg, H.; McCloskey, A. L., Eds.; Macmillan: New York, 1964; Vol I, Chapter 2.
(5) Schaeffer, R.; Tebbe, F.; Phillips, C. *Inorg. Chem.* **1964**, *3*, 1475.